Available online at www.sciencedirect.com

ScienceDirect

International Journal of Solids and Structures 44 (2007) 4690–4706

INTERNATIONAL JOURNAL OF SOLIDS and STRUCTURES

www.elsevier.com/locate/ijsolstr

Imperfection sensitivity of pyramidal core sandwich structures

Russell Biagi, Hilary Bart-Smith *

Department of Mechanical and Aerospace Engineering, University of Virginia, Charlottesville, VA 22904, USA

Received 21 July 2006; received in revised form 27 November 2006
Available online 5 December 2006

Abstract

Lightweight metallic truss structures are currently being investigated for use within sandwich panel construction. These new material systems have demonstrated superior mechanical performance and are able to perform additional functions, such as thermal management and energy amelioration. The subject of this paper is an examination of the mechanical response of these structures. In particular, the retention of their stiffness and load capacity in the presence of imperfections is a central consideration, especially if they are to be used for a wide range of structural applications. To address this issue, sandwich panels with pyramidal truss cores have been tested in compression and shear, following the introduction of imperfections. These imperfections take the form of unbound nodes between the core and face sheets—a potential flaw that can occur during the fabrication process of these sandwich panels. Initial testing of small scale samples in compression provided insight into the influence of the number of unbound nodes but more importantly highlighted the impact of the spatial configuration of these imperfect nodes. Large scale samples, where bulk properties are observed and edge effects minimized, have been tested. The stiffness response has been compared with finite element simulations for a variety of unbound node configurations. Results for fully bound cores have also been compared to existing analytical predictions. Experimentally determined collapse strengths are also reported. Due to the influence of the spatial configuration of unbound nodes, upper and lower limits on stiffness and strength have been determined for compression and shear. Results show that pyramidal core sandwich structures are robust under compressive loading. However, the introduction of these imperfections causes rapid degradation of core shear properties.

Keywords: Cellular metals; Pyramidal lattice; Failure modes; Sandwich panels; Imperfections

1. Introduction

Sandwich construction has been revolutionized by the introduction of a new class of lightweight metallic cores. This has been due to significant advances in the design and fabrication of these structures (Wadley et al., 2003; Zok et al., 2003). These panels use a variety of truss, prismatic, and textile cores, which are attached to stiff face sheets. This material arrangement produces a structure with greater bending stiffness than that of a solid plate of equal mass (Allen, 1969). Recent analysis has demonstrated that they can compete on

* Corresponding author.
E-mail address: hb8h@virginia.edu (H. Bart-Smith).

0020-7683/$ - see front matter
doi:10.1016/j.ijsolstr.2006.11.049

mechanical performance with current industry standards, such as honeycomb cores (Evans et al., 2001; Chiras et al., 2002). One critical advantage that these new cores have is that they present the opportunity to add functionality to the panels, such as thermal management, energy absorption, and morphing capabilities (Gu et al., 2001; Fleck and Deshpande, 2003; Rathbun et al., 2005).

Before these sandwich panels can be implemented as structural components in the field, it is necessary to examine and quantify their sensitivity to imperfections on stiffness and load capacity. For example, the mechanical performance of a structure if debonding takes place between the core and faces needs to be understood. The sandwich effect—i.e. improved bending stiffness at lower mass—is lost if bonding between the core and face is compromised to such an extent that sliding of the two faces over one another takes place. When one considers a truss core structure, where the "bond" is a series of discrete nodes bonded to the face, it is essential that the influence of unbound nodes on mechanical performance be understood. With this motivation, compression and shearing have been chosen as the testing methods to explore this issue. The bond imperfections are introduced to samples during the fabrication process. These flaws are expected to affect the stiffness and load capacity. By measuring the stress–strain responses on imperfect panels, and comparing with those for "pristine" panels, the extent of the degradations in mechanical properties can be explored.

There have been a number of studies that report on the mechanical performance and multifunctionality of lattice truss structures and show that they have superior stiffness-to-weight performance (Christensen, 2000; Deshpande and Fleck, 2001; Deshpande et al., 2001; Wallach and Gibson, 2001; Wicks and Hutchinson, 2001, 2004; Chiras et al., 2002; Wadley et al., 2003; Sugimura, 2004; Zok et al., 2004; Queheillalt and Wadley, 2005a,b). Several publications have mentioned the fact that imperfections can inhibit the performance of the core (Evans et al., 1998, 2001; Wadley et al., 2003) but there has been little follow up analysis on this topic. Deshpande et al., introduced ligament curvature to an octet truss and found that shape imperfections knockdown the collapse stress as the structure goes from being stretch dominated to bending dominated (Deshpande et al., 2001). This result is similar to cell wall curvature studies of honeycomb cores that demonstrated performance degradation by decreasing the buckling load (Chen et al., 1999, 2001). Wallach and Gibson (2001) presented an imperfection analysis in which members were removed from a truss structure similar to an octet truss. They found that the compressive modulus and strength of the structure decreased linearly with the fraction of ligaments removed. Uniform truss member thinning also produced a linear reduction in stiffness and strength, at a rate of approximately 0.6 times that for an equivalent density reduction by removing members (Wallach and Gibson, 2001). It should be noted that this study involves the removal of material from the structure, thereby decreasing its relative density. Studies have also noted that the compressive and shear properties of a cellular core can be influenced by its interaction with the face sheets (Bart-Smith et al., 2001; Wallach and Gibson, 2001). Defects that reduce the mechanical performance without significantly reducing the relative density of the structure are a clear possibility in truss core sandwich panels and must be investigated.

The paper is organized in the following way. Section 2 gives an overview of mechanical response predictions for a pyramidal core sandwich panel with no imperfections. Section 3 details the core and panel fabrication. Sections 4 and 5 present details of the experimental and simulation techniques used to determine the compressive and shear response of the sandwich panels. The results for the experiments and simulations are presented and discussed in Section 6. Section 7 gives the conclusions and provides a brief description of future work.

2. Mechanical behavior predictions

The core must serve several functions vital to the mechanical performance of sandwich structures. It must, (i) maintain the correct separation between the face sheets, (ii) be stiff enough in shear to prevent the face sheets from sliding past one another, and (iii) keep the faces nearly flat (Allen, 1969). Core topology and relative density along with face sheet properties govern the panel failure mode. With strong face sheets available and for minimum weight designs, panel performance is driven by the core properties (Allen, 1969; Zok et al., 2004).

The following analytical expressions have been developed by Deshpande and Fleck for the pyramidal lattice truss composed of elastic-perfectly plastic and strain hardening materials (Deshpande and Fleck, 2001). The predictions for stiffness and strength assume the core struts to be individual axially loaded columns to simplify the analysis.

The relative density, $\bar{\rho}$, of the lattice truss is the ratio of the unit density, ρ^*, to the solid from which it is made, ρ_s, or equivalently the volume fraction of truss members occupying the unit cell. For a pyramidal core with square cross section ligaments the relative density is

$$\bar{\rho} = \frac{\rho^*}{\rho_s} = \frac{2}{\cos^2(\omega)\sin(\omega)}\left(\frac{t}{l}\right)^2, \tag{1}$$

where ω is the included angle (see Fig. 1), t is the thickness of the ligaments, and l is the strut length.

The out-of-plane compressive stiffness, E_{33}, is given by

$$E_{33} = E_s\bar{\rho}\sin^4(\omega), \tag{2}$$

where E_s is the Young's modulus of the parent alloy and $\bar{\rho}$ is the relative density given in Eq. (1). The shear stiffness, G_{31}, has the form

$$G_{31} = E_s\frac{\bar{\rho}}{8}\sin^2(2\omega). \tag{3}$$

Deshpande and Fleck (2001) also derived the compressive and shear strengths for a pyramidal truss core. If the pyramidal truss composed of an elastic-strain hardening material then it can fail by plastic buckling. Specifically, the compressively loaded truss material begins to yield but is able to support increased load due to strain hardening effects. In this case the truss members fail (plastically buckle) at the bifurcation strength, σ_{cr}, given by Shanley–Engesser tangent modulus theory (Shanley, 1967),

$$\sigma_{cr} = \frac{k^2\pi^2 E_t}{12}\left(\frac{t}{l}\right)^2, \tag{4}$$

where k is a dimensionless factor that depends on the rotational stiffness of the end nodes (i.e. $k = 1$ or $k = 2$ for pinned and built in ends respectively) and E_t is the tangent modulus, defined by the slope, $d\sigma/d\varepsilon$, of the uniaxial stress versus strain curve of the parent material at a stress level σ_{cr}. A value of $k = 2$ is assumed appropriate to model ligaments with brazed ends. The peak compressive strength for a lattice truss is given by

$$\sigma_{33}^{pk} = \frac{k^2\pi^2}{24}\sin^3(\omega)\cos^2(\omega)E_t\rho^2. \tag{5}$$

Due to symmetry, the in-plane shear strength for the pyramidal lattice truss has a periodicity of $\pi/4$ with respect to the loading orientation angle ψ (Fig. 1) resulting in a minimum and maximum. The cores were loaded in the 3-1 orientation ($\psi = 0$), shown in Fig. 1, which is the loading orientation giving the maximum shear response. This orientation was chosen primarily for ease of sample manufacturing. The failure mechanism observed experimentally was plastic buckling of adjacent truss ligaments. For a strain hardening material the peak stress is given by

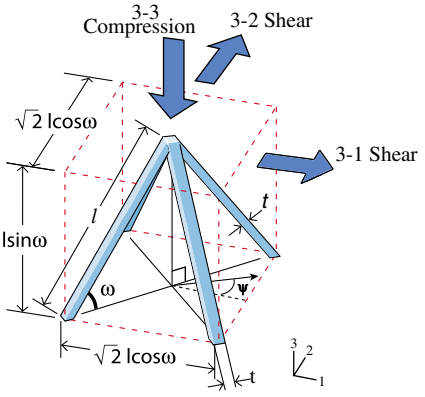

Fig. 1. Schematic of a pyramidal unit cell with included angle (angle from a ligament to the base) ω, ligament length, l, and square cross section thickness, t.

$$\sigma_{31}^{pk} = \frac{\sqrt{2}}{4}\sigma_{cr}\bar{\rho}\sin(2\omega). \quad (6)$$

In this paper, experiments and simulations have been developed to probe the affect of unbound nodes from the face sheet on the mechanical performance of the pyramidal truss core. The analytical predictions described here will be used as a comparison to "perfect" cores (cores without introduced imperfections) only, since they do not take into account the influence of defects.

3. Materials and manufacture

The pyramidal cores are made using commercially available 304 stainless steel (Fe–18Cr–8Ni). In order to control imperfections within pyramidal core sandwich panels, it is essential to create pristine samples with all nodes bound to the face sheets. Adapting techniques developed by others, diamond perforations were laser cut into a flat 1.22 mm thick sheet of 304 stainless steel producing uniform square cross section ligaments for all of the cores (Sypeck and Wadley, 2002). The flat perforated sheet was folded along successive node rows using a CNC operated punch and die tool forming regular pyramids with consistent bend angle, illustrated in Fig. 2. During the folding process, the perforated sheet was held in place by a fixture to ensure proper node alignment. The result was a core of regular pyramids with an angle $\omega = 45 \pm 2°$ (see Fig. 1 for definition of ω) and predicted relative density $\bar{\rho} = 0.046$ or 4.6% (Eq. (1)). The measured pre-braze relative density of these cores was $\bar{\rho} = 0.035 \pm 0.002$. The discrepancy is due to "double counting" the nodal volume in the expression for the predicted relative density (Deshpande and Fleck, 2001). A photograph of a pyramidal core fabricated using this technique is shown in Fig. 2b.

Sandwich panels were created by securing a bent pyramidal truss core between two 304 stainless steel sheets using a brazing process. The nodes or apexes of the pyramids of the truss cores were successively dipped in a polymer based binder (Nicrobraz® 520 Cement) and a Nickel based metallic braze powder, Ni–22Cr–6.5Si–4.5P (Nicrobraz® 31), both supplied by Wall Colmonoy Corporation (Madison Heights, MI). Only the nodes were dipped in order to regulate the amount of braze and more importantly, control which nodes would be bound to the face plates and which would be left free, or unconstrained, to simulate an imperfection. A simple, low tech method was employed that allowed the "imperfect" nodes to be protected from braze during the dipping process. Masking tape was placed over the nodes that were to be free of braze and the core was dipped in the binder and braze powder. The masking tape was then removed from the selected nodes exposing a clean, braze free surface. These nodes were then painted with Stop-Off™ (Wall Colmonoy Corp., Madison Heights, MI), a material designed to protect metal surfaces from molten braze material and prevent metal surfaces from adhering to each other at high temperatures. This insures nodes will not adhere to the face sheets. The dipped truss core was placed between two 304 stainless steel face sheets (1.5 mm thickness for compression, 3.35 mm

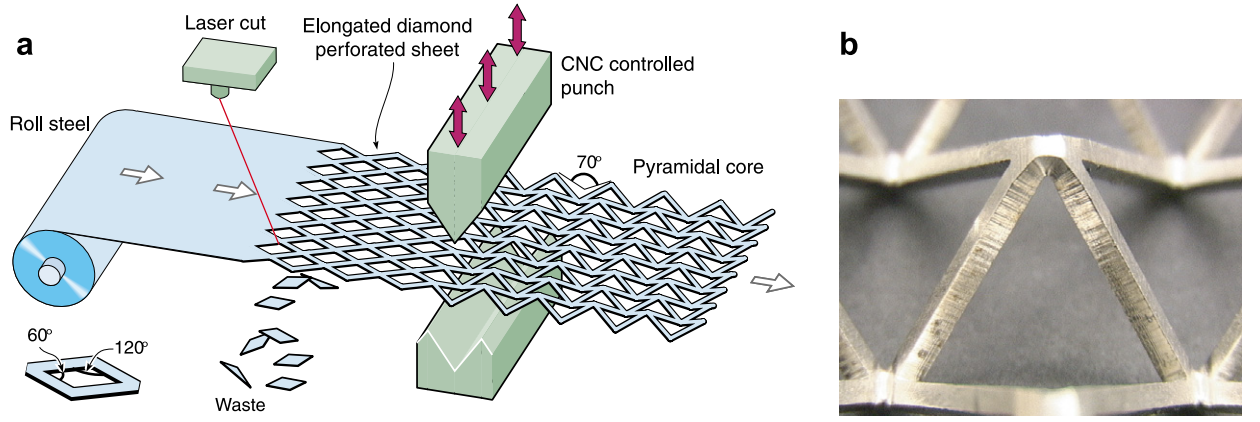

Fig. 2. (a) Illustration of the perforation and bending process used to manufacture the pyramidal core. (b) Photograph of a pyramidal core laser cut and CNC bent resulting in consistent nodes and square cross section ligaments.

thickness for shear) and placed in a vacuum furnace. At a pressure of $\sim 10^{-4}$ torr, the samples were heated at 10 °C/min to 550 °C and held for 1 h to volatilize the binder material. The temperature was then increased to 1050 °C and held for 1 h to allow the braze material to liquefy. The samples were then furnace cooled to ambient temperature leaving the samples in an annealed state. The relative densities of the brazed specimens will be discussed in Sections 4.1 and 4.2.

4. Experiment

Samples were tested in compression and shear following ASTM C 365-00 and ASTM C 237-00 guidelines, respectively for sandwich panels (ASTM, 2000; ASTM, 2000). A screw driven testing machine (Model 4208, Instron Corporation, Canton, MA) was used to test these samples at an applied strain rate of 10^{-3} s^{-1}. Engineering strain was measured using retro reflective tape and a laser extensometer (Model LE-05, EIR Ltd., Irwin, PA) with accuracy of ± 0.005 mm. A 300 kN load cell (accuracy of $\pm 0.5\%$) measured the force that was used to calculate the stress on the core. During the compression experiments, frictional forces were assumed to be sufficient to restrict lateral movement and the cores were not constrained in the direction normal to the applied load.

Initial tests were performed on small scale samples to gain some insight into the influence of these imperfections (Biagi, 2006). Ashby et al. state that, for compression testing, boundary effects become negligible when the ratio of specimen size to cell size is greater than about 7 (Ashby et al., 2000). The small scale samples tested here were well below this ratio and therefore dominated by edge effects. However, they were used to gain insight into the mechanical behavior of these structures in the presence of imperfections and highlight areas of importance other than simply unbound node number, such as unbound node connectivity.

4.1. Compression

To minimize edge effects, large scale compression samples were square cores containing 49 cells. This was the maximum sample size that would fit comfortably on the 150 mm diameter steel load platens of the testing machine. Varying percentages of nodes—from 0% to 90%, in intervals of 10%—were chosen to be unbound with a random configuration. The configuration of the unbound nodes at each percentage was chosen at random using a random number generating program written in MatLab®. Three tests were performed at each percentage of unbound nodes with all three samples having the same nodal configuration.

After fabrication of the sandwich panels, post-braze relative densities varied with the percentage of unbound nodes. Table 1 lists the measured post-braze relative densities for all nodal configurations. The added braze material minimizes the discrepancy between predicted and measured relative density at lower percentages of unbound nodes, where the amount of braze added to the core is proportionately large. Experimental data normalizations are based on the measured post-braze relative densities (Table 2).

Table 1
Measured post-braze relative densities for pyramidal core sandwich panels tested in compression, with predicted relative density $\bar{\rho} = 0.046$ and measured pre-braze relative density $\bar{\rho} = 0.035$

Percent of nodes unbound	Post-brazed measured relative density
0	0.041 ± 0.002
10	0.040 ± 0.002
20	0.041 ± 0.003
30	0.040 ± 0.004
40	0.039 ± 0.001
50	0.039 ± 0.001
60	0.037 ± 0.004
70	0.036 ± 0.001
80	0.037 ± 0.002
90	0.036 ± 0.002

Table 2
Measured post-braze relative densities for pyramidal core sandwich panels tested in shear, with predicted relative density $\bar{\rho} = 0.046$ and measured pre-braze relative density $\bar{\rho} = 0.035$

Percent of nodes unbound	Post-brazed measured relative density
0	0.042 ± 0.001
10	0.040 ± 0.001
20	0.040 ± 0.002
30	0.039 ± 0.002
40	0.040 ± 0.001
50	0.040 ± 0.002
60	0.039 ± 0.003
70	0.039 ± 0.001
80	0.037 ± 0.003
90	0.036 ± 0.001

4.2. Shear

For minimum weight sandwich beams (i.e. structures with thin face sheets), the core is responsible for the shear stiffness of the beam, preventing relative translation of the face sheets (Allen, 1969). The shear properties govern several failure modes such as transverse shear failure of a beam in bending and general buckling and shear crimping of a beam in in-plane compression (Bitzer, 1997). Compression shear experiments were performed on cores containing 60 cells (12 cells $\times$ 5 cells). The size of the shear specimens was dictated by ASTM C 237-00 guidelines, which states that the sample must have a minimum length to thickness ratio $L/T > 12$ (ASTM, 2000). If the sample is relatively long compared to the thickness, the specimen is loaded in almost pure shear (Ashby et al., 2000). All samples tested in this study had a ratio $L/T \approx 17$. The configuration of unconstrained nodes was chosen the same way as for the compressive samples. As with the compression samples, the measured post-braze relative density varied slightly due to the quantity of braze material.

Three tests were performed for each configuration. To ensure that the specimen was adequately attached to the shear platens, a configuration of 22 holes total were drilled and tapped in the face sheets allowing them to accept screws (#10–32) secured through the loading plates. There was also a ridge at the leading edge of each shear plate to further secure the sandwich panel. A schematic of the core and shear loading plates is shown in Fig. 3.

5. Simulation

Numerical simulations were performed for both compression and shear tests using the Abaqus/Standard general-purpose finite element program (Hibbitt, Karlsson & Sorensen, Inc., Providence, RI). The simulations are used to evaluate and probe upper and lower bounds on the mechanical properties of the panels. A convergence study was performed to ensure that a mesh was chosen that gave an accurate result within a reasonable calculation time.

To study the response of imperfect samples numerically, quadratic beam elements in space (B32) or Timoshenko shear flexible beams were used to model the core, shown in Fig. 4. Due to the discrete nature of the nodal imperfection, it was necessary to model the individual truss elements, rather than using a continuum model to represent the core as done by Xue and Hutchinson, 2004. Beam elements are a one dimensional approximation of a three dimensional continuum and much less costly than continuum elements themselves (Abaqus, 2002). For transverse shear flexibility to be negligible, the thickness of a ligament should be less than 1/15 of the ligament length (Abaqus, 2002). This proportion is known as the slenderness ratio. The cores tested had a slenderness ratio of approximately 1/11 which prevented the use of Euler–Bernoulli beam elements. If the beam is slender, the shear deformation is negligible. In shear flexible beam theory, plane sections initially normal to the axis of the beam do not necessarily remain plane as deformation occurs. The performance of the beam elements has been evaluated and is comparable to the continuum simulations (Biagi, 2006).

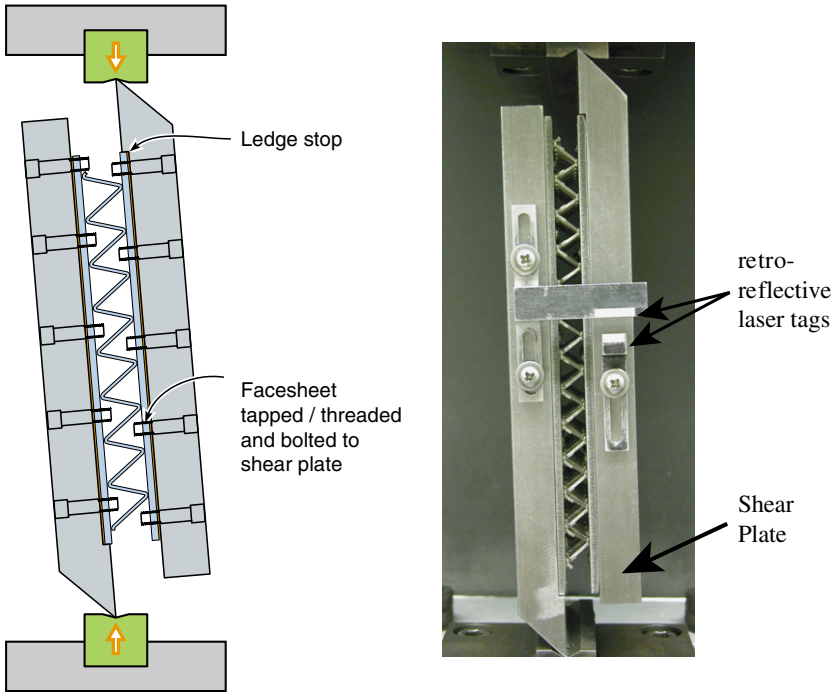

Fig. 3. Schematic of a compression shear fixture (left) and picture of an experimental shear test. The tabs on the front of the experimental core hold the retro-reflective laser tags used by the extensometer.

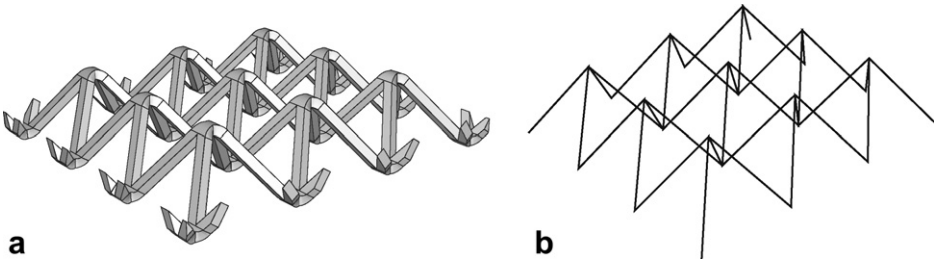

Fig. 4. (a) Three dimensional model of a 9-cell core used for small scale simulations that was meshed with continuum elements. (b) Wire model of a 9-cell core that was meshed using beam elements.

For a core with all nodes constrained to the face sheet the model gives results through the plastic region—the results of these simulations are compared with the analytical predictions. However, it was not possible to simulate the yield and post yield behavior of the imperfect samples. The introduction of randomly distributed unconstrained nodes created a numerical instability that prevented the determination of the post yield behavior. As a result, only elastic properties were characterized by the simulations.

In order to replicate the compression and shear experiments, the simulations had the same unconstrained nodal configurations. For this analysis, it is necessary to define appropriate boundary conditions to model either a perfect or imperfect bond between nodes and face sheet. Out-of-plane compression simulations were performed either on a core alone, with displacement boundary conditions placed directly on the nodes, or on a core between two rigid face sheets to which the displacement was applied. There was no friction present in either model. The results were identical and, for simplicity, all data presented is for analyses performed without face sheets. Nodes bonded to the face sheets experienced fixed boundary conditions; i.e. were restricted from all translation and rotation. The vertical translation constraint was relaxed for bound top nodes to allow the imposed displacement necessary for compression. Unbound base nodes were only constrained vertically while unbound top nodes were free in plane and had a prescribed vertical displacement.

For the shear simulations, bound base nodes were fixed from translating and rotating and bound top nodes were allowed to translate in the 1- and 3-directions. A vertical constraint was applied to unbound base nodes while unbound top nodes were left completely free. It should be noted that for the imposed core shear conditions explained in Section 4.2, bound top nodes experience an in-plane displacement in the direction of shear and all top nodes undergo an out-of-plane displacement. However, only small shear strains were applied in the simulations, up to a maximum of 0.2%, resulting in a negligible out-of-plane strain of 0.0002%. This allowed the unbound top nodes to be free of any vertical displacement with a negligible effect on the mechanical response. A displacement boundary condition was applied in the 1-direction to all bound top nodes (see Fig. 1).

6. Results and discussion

Results from compression and shear tests are presented. Tests were performed to obtain the mechanical response of the parent material. Stiffness characteristics were obtained via numerical methods and compared with the experimental findings. As stated previously, the introduction of unbound nodes created a numerical instability that prevented the simulation of the yield and post yield characteristics of an imperfect core. Therefore, only the experimental post yield findings are presented.

6.1. Parent material response

The parent material constitutive response is needed for the analytical predictions of Section 2 and as an input for the finite element simulations. The Young's modulus, E_s, yield stress, σ_y, and tangent modulus, E_t, can be found through direct measurement of the stress vs. strain results, or by fitting a Ramberg–Osgood relation to the tensile test curve. The Young's modulus and yield stress were found directly from the stress–strain response of the tests performed. The Ramberg–Osgood relation was fit to the average tensile data to find the tangent modulus, E_t, needed to compute the truss member bifurcation stress, $\sigma_{cr}(E_t)$.

Tension tests were performed on two specimens. The cores used were manufactured from two separate stocks of type 304 stainless steel. Core stiffness and strength can be normalized by the relative density and material properties as a way to examine and compare core topologies (Ashby et al., 2000). Fig. 5 shows the stress vs. strain response for both materials tested. Table 3 gives the data obtained from graphs using the conventional 0.2% offset to find the yield stress.

It should be noted that the samples were coated with a very thin layer of Nicrobraz® 31 braze powder prior to the thermal cycle. This was done to obtain material properties that would closely resemble those of a core in a sandwich panel. The braze can influence the response of the material, which increases with braze concentra-

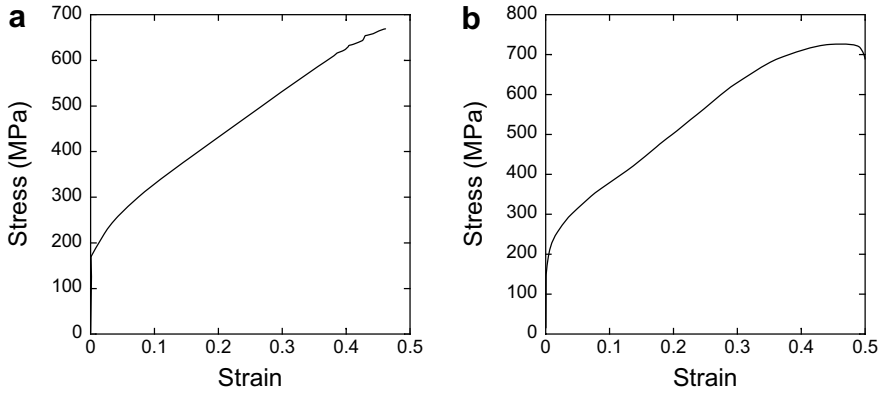

Fig. 5. The uniaxial stress versus strain response of two samples 304 stainless steel. Both samples were lightly coated with braze material and put through the same thermal cycle used for sandwich panel fabrication.

Table 3
Measured modulus and yield stress (0.2% offset) properties for two samples of 304 stainless steel coated with Nicrobraz® 31 braze material and heated at 1050 °C for 60 min

	Yield stress (MPa)	Elastic modulus (GPa)
Sample A	174	191
Sample B	179	208

tion, as noted by Zok et al. (2004). Braze concentration and spatial distribution is not consistent for each sample, contributing to the material property discrepancy.

6.2. Compression

Three samples, having the same unbound node configuration, were experimentally tested at each percentage and the average compressive stiffness, E_{33}, and peak strength, σ_{33}^{pk}, are reported. These structures exhibit a response that is analogous to that described for small scale samples tested in compression (Biagi, 2006). There is a brief period of node bedding followed by a linear elastic response until core yield. The panel continues to support increasing load due to strain hardening effects in the core struts until peak stress. This is followed by a softening of the core until densification. There was no node rupture observed for any compression experiments performed.

6.2.1. Stiffness assessment

The preliminary study of small scale samples indicated that given the same number or percentage of unbound nodes, the mechanical response can vary if their locations vary (Biagi, 2006). This suggests that there are upper and lower limits to the response depending on the nodal configuration. Percolation theory has been suggested as a way to possibly understand defects in honeycomb structures (Gibson and Ashby, 1997). Adapting this concept to unbound nodes within a lattice truss, percolation theory deals with "clusters" of unbound nodes and pathways of imperfections. A critical pathway occurs when a there is a continuous path of unbound nodes from one side of the core to the other (Stauffer and Aharony, 1992; Grimmett, 1999). This suggests that the edge nodes play a significant role in the mechanical response of a core in compression. A continuous pathway from one edge to another is unattainable if the edge nodes remain bound to the face sheets (Fig. 6), maintaining an equiaxed force on all interior nodes. Therefore, it can be reasoned that as long as the edge nodes

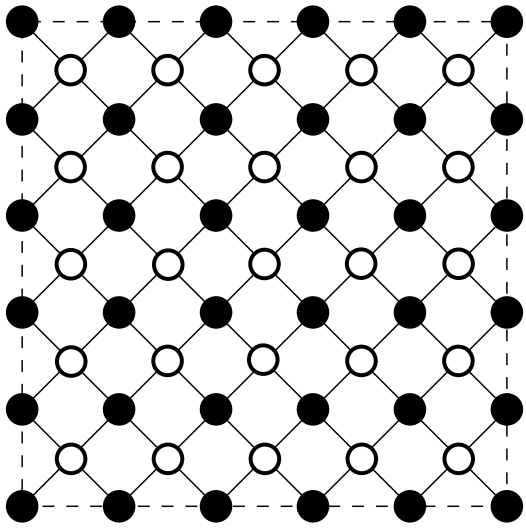

Fig. 6. Illustration of node connectivity for a pyramidal lattice truss. Solid circles denote base nodes, hollow circles are top nodes and solid lines are truss ligaments connecting the two. The dashed line indicates the edge nodes on the perimeter.

remain fixed, any percentage of interior nodes can be unbound with little effect on the core performance, creating an upper bound.

At a critical value, the percentage of unbound nodes, N, will become too great to remain only in the interior of the core. For a square pyramidal core, the critical percentage can be expressed mathematically as

$$N_{\text{critical}} = \frac{2n(n-3)+5}{2n(n-1)+1}, \tag{7}$$

where n is the number of edge nodes on one side of the core. This formula is specific for a square perimeter pyramidal truss core and would vary depending on core topology and panel geometry. For the compression cores tested here, $N_{\text{critical}} = 75\%$. The lower limit was taken to be the inverse of the upper bound configuration, with perimeter nodes unbound first. Selecting unbound nodes on the perimeter reduces the number of nodes experiencing an equiaxed force, resulting in a minimum stiffness response.

Finite element simulations were conducted to probe the stiffness limits at each percentage of unbound nodes (in increments of 10%). At each percentage, ten simulations were performed—eight configurations were randomly generated while two probe the upper and lower limits. Fig. 7 shows a plot of the normalized modulus, $E_{33}/(E_s\bar{\rho})$, versus number of unbound nodes, calculated from the simulations.

For a pristine core (no unbound nodes) the simulation and analytical prediction are within 2%. The upper bound results confirm that if the edge nodes remain bound the compressive stiffness remains constant. In essence, bound edge nodes resist lateral expansion of the core and maintain an equiaxed force on interior core nodes. When an edge node is unbound and there is a pathway of imperfections to an edge, the stiffness declines. The lower limit follows a linear trend. The compressive modulus of all cores with randomly generated unbound node configurations falls within the upper and lower bounds.

Experiments and simulations were carried out on cores with the same configuration of unbound nodes. The modulus was measured experimentally by loading the core into the plastic range and using the slope of an unload curve, following protocols developed by Ashby et al. (2000). The unload curve at 4% strain is used here. The comparison is shown in Fig. 8. For a fully bound core, the experiment, simulation, and analytical prediction are in excellent agreement. Both the experimental and simulation results indicate that there is virtually no decrease in stiffness at the 10% unbound node configuration. Simulations and experiments (within deviation) show that even when 20% of the nodes are unbound, the core modulus is within 10% of a perfect core. In addition to this, looking at the eight randomly generated 20% unbound node orientations simulated in compression (Fig. 7), the most compliant response differed by 11% from the upper bound. These results suggest that the compressive stiffness of the pyramidal core has reasonable tolerance to unbound nodes.

Initially the experiment and simulation are in good agreement. However, at larger percentages of unbound nodes, the measured response indicates that the modulus is higher than predicted. A possible explanation for this discrepancy is nodal stiffness. The lower bound (Fig. 8) suggests that when all core nodes are unbound

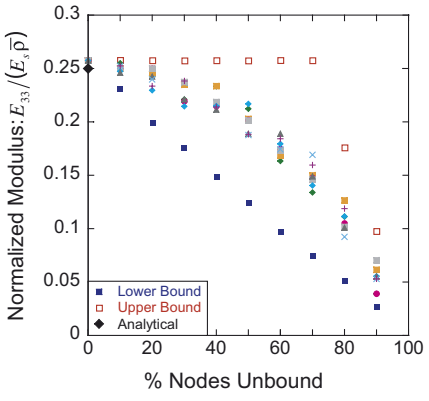

Fig. 7. Simulation results for the normalized compressive stiffness. The upper and lower bound are probed at each percentage along with eight randomly generated nodal configurations.

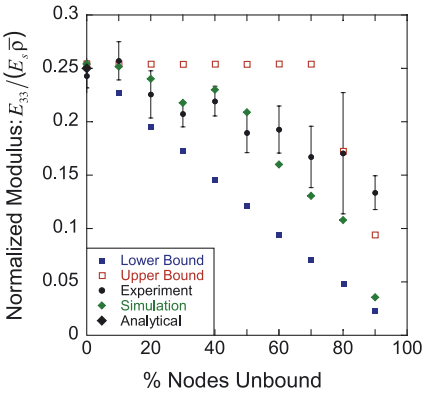

Fig. 8. Numerical and experimental compressive modulus comparison. (Error reported as ± one standard deviation).

from the face sheets (i.e. no nodes are constrained and all sandwich panel properties are lost) the stiffness response of the core itself is zero, or the structure becomes a mechanism in the absence of nodal constraints. However, even if a core was compressed on a frictionless surface there would be a measured mechanical response due to the inherent stiffness of the material that forms the nodes. Recall that the truss ligaments were modeled using beam elements where nodes (ligament intersections) are points. Once nodes are unconstrained the model lacks nodal material to provide the rotational stiffness at the truss ends present in the physical cores. This becomes more pronounced as the percentage of unbound nodes increases and is the primary source of the stiffness discrepancy.

Another possible explanation for the stiffness discrepancy at high unbound node percentages is the lack of friction in the simulations. When a large number of nodes are unconstrained, say greater than 60%, the frictional forces may have a sizeable impact on the panel response. However, when there are a small number of unbound nodes in the core, the contribution of frictional forces to the overall response is minimal.

6.2.2. Peak compressive stress

Fig. 9 shows the normalized peak compressive stress data for pyramidal core panels in the presence of unbound nodes. For a perfect core, the analytical and numerical predictions are in very good agreement. The experimentally determined peak stress is slightly higher that the predictions by approximately 20%. Similar discrepancies have also been reported elsewhere and these are caused by inconsistencies in material mechanical properties (Zok et al., 2004). Specifically, the braze material has been shown to increase the flow stress of the alloy which contributes to the strain hardening effect.

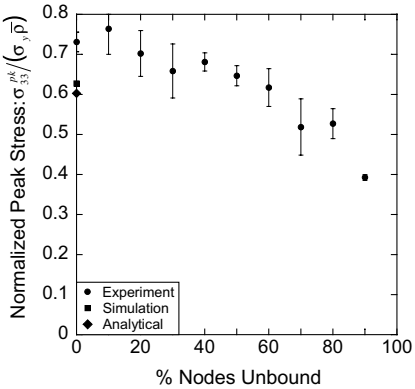

Fig. 9. Measurements of peak compressive stress (±one standard deviation). The plastic buckling prediction for a perfect core assumes a fixed truss ligament end constraint (k=2).

The results show that a pyramidal core sandwich panel, subject to compressive loads, is able to retain its load capacity in the presence of unbound nodes. At low percentages of unbound nodes—up to approximately 20%—the peak strength is not significantly impacted. As the number of unbound nodes increases, there is a gradual decline in the peak stress. It is interesting to note that at 90% unbound nodes, the sample is still able to retain almost half of the load capacity attained for a perfectly bonded core.

6.3. Shear

Three samples were tested in the 3–1 direction (see Fig. 1) at each unbound node configuration and the shear stiffness and peak stress are reported. Fig. 10 shows stress vs. strain curves for a pyramidal core in shear with 0% and 20% unbound nodes. Initial loading appears elastic until core yield is reached. The cores were observed to continue to support load through a gradual strain hardening until a peak stress was reached or node rupture occurred, Fig. 11. This load orientation places two adjacent unit cell ligaments in compression and the other two in tension. Plastic buckling of truss ligaments in compression was the observed failure mechanism. Node rupture occurred on most cores at a strain of approximately 20%. It is clear from Fig. 11 that the ligaments corresponding to the unbound node do not deform and no longer contribute to the shear response.

6.3.1. Stiffness assessment

Experimental and simulation results are presented in Fig. 12. The simulations are in excellent agreement with the experimental results for all tests other than the fully bound configuration. For the perfect sample, the simulation and analytical calculations over predict the experimentally determined modulus. The influence of the braze material could contribute to this small discrepancy. It was also observed that the fully bound cores experienced a larger compressive strain than the other cores tested. Following the ASTM C 237-00 guidelines, the cores were not in pure shear. However, the compressive force is negligible compared to the shear force.

The results indicate that the shear stiffness is greatly affected by the presence of unbound nodes. For cores in compression all nodes experience a compressive force that is transferred to the related struts, whether they are bound or unbound. Bonding the nodes only prevents lateral movement, making edge nodes most important. For a core in shear, the force is transmitted from the face sheets to the core through the braze material. When braze material is removed, force is no longer transmitted to the node and the four connected ligaments no longer contribute to the response—Fig. 11 clearly highlights this. Unlike cores in compression, there is no way to restrict the pathway of the mechanism.

Each node that is unbound affects a certain volume or area fraction of the core, leaving only an "effective area" contributing to the response. The effective area, A_{eff}, can be expressed as

$$A_{\text{eff}} = A_{\text{total}} - \eta A_{\text{unit}}, \tag{8}$$

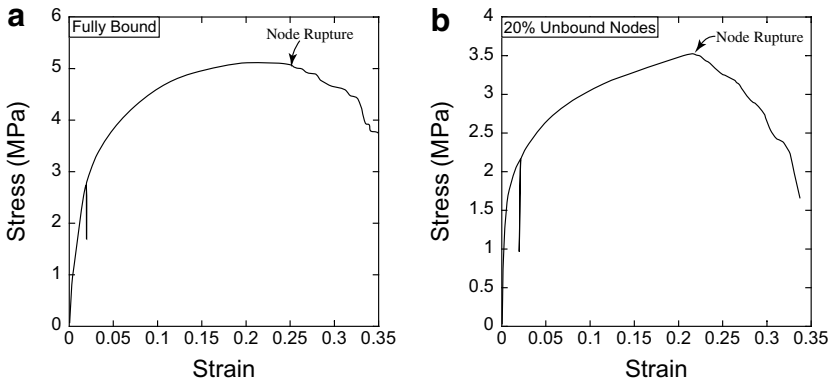

Fig. 10. Representative shear stress–strain responses for a pyramidal core with node rupture occurring at large strains subsequent (a) and prior (b) to peak stress.

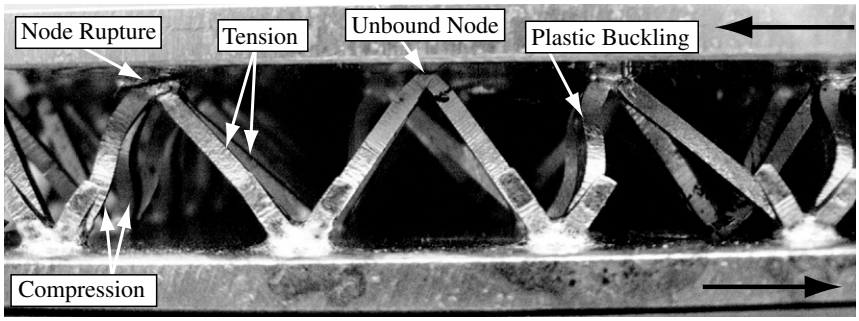

Fig. 11. Picture of a pyramidal core in 3–1 shear. Plastic buckling occurs while ligaments attached to the unbound node do not deform. Node rupture is observed at large strains.

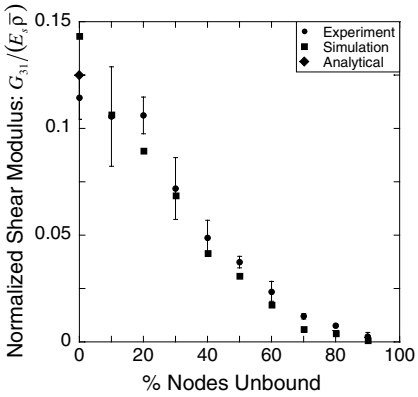

Fig. 12. Experimental and simulation results for shear modulus of a pyramidal core loaded in the 3–1 direction (1). (Experimental error reported as ± one standard deviation).

where A_{total} is the total area of the core, A_{unit} is the area of a unit cell, and η is a weight function that is dependent on the number and orientation of unbound nodes. An unbound interior node affects the area of one unit cell (A_{unit}) while an unbound edge node and corner node affect half ($A_{\text{unit}}/2$) and a quarter ($A_{\text{unit}}/4$) of a unit cell area, respectively (Fig. 13). Orientation becomes important when adjacent base and top nodes are unbound and affected areas overlap. This overlap would lead to an overestimation of affected area if it were not taken into account.

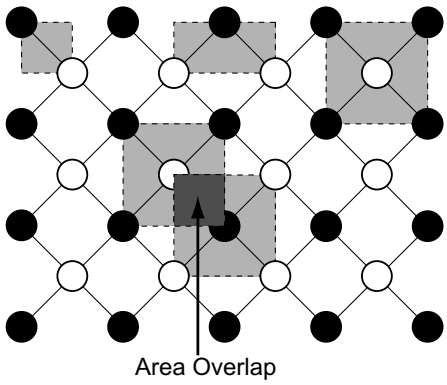

Fig. 13. Diagram representing the affected area (light gray highlight) for an interior, edge, and corner node and the overlap (dark gray highlight) of affected area that can occur. Solid circles represent base nodes and hollow circles represent top nodes.

To describe this weight function analytically is problematic due to the inherent complexity of nodal interactions. For each core, the effective area can be calculated through inspection or numerically, following the area guidelines given above. The affect of imperfections is calculated by multiplying the response for a fully bound core by the effective area ratio, $A_{\text{eff}}/A_{\text{total}}$. Using the simulation data, the modulus for the perfect core was multiplied by the effective area ratio for each node configuration tested and compared to the model. The results are shown in Fig. 14.

The area assumption follows the same trend as the simulation and they are in good agreement. Consequently, the upper and lower bounds correspond to the maximum and minimum effective area remaining, respectively. The minimum area affected by these imperfections—thereby giving the upper bound—is given by alternating unbound nodes between face sheets, starting with the corner nodes and working inward toward the center trying to maximize unbound node interaction. The maximum core area affected occurs if successive nodes along a single face sheet are unbound first (i.e. all top nodes), producing the lower bound. The bounds are shown in Fig. 15 along with the other stiffness results obtained.

The results show that even the upper bound constitutes a significant degradation in shear stiffness with the introduction of unbound nodes. Both limits follow a linear trend in the reduction of shear stiffness. The lower bond shows that at 43%, all top nodes are unbound and shear force is no longer transmitted to the core. Slight perturbations from linearity may be the result of asymmetries of node orientation. Note that the node orientations to obtain the limits were chosen by inspection but are believed to be the bounds based on the reasoning above.

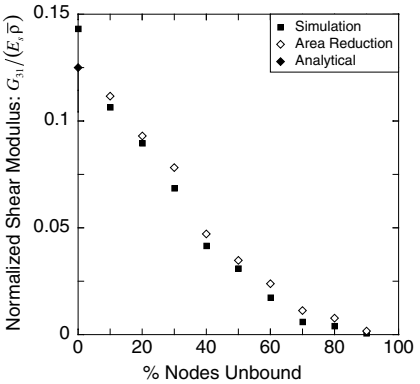

Fig. 14. Normalized modulus comparison between simulations and estimation using effective area ratio. For this method the simulated modulus for the perfect core was multiplied by the ratio of effective area to total area at each unbound configuration.

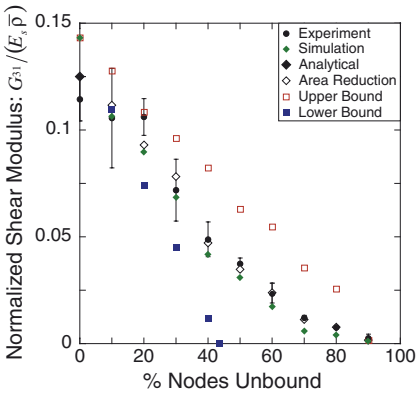

Fig. 15. Normalized shear modulus results with upper and lower bound estimations. The upper and lower bounds were obtained by affecting the minimum and maximum core area, respectively, with unbound nodes.

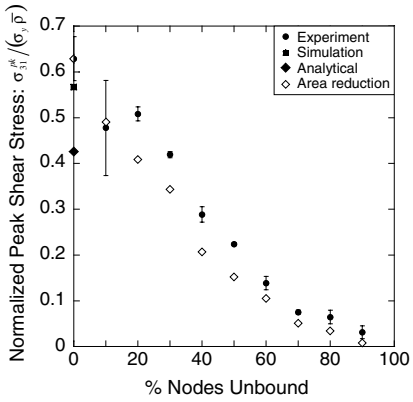

Fig. 16. Normalized peak shear strength for a pyramidal core (± one standard deviation). The analytical value assumes fixed strut end conditions ($k = 2$). The area reduction estimation uses the initial measured peak stress.

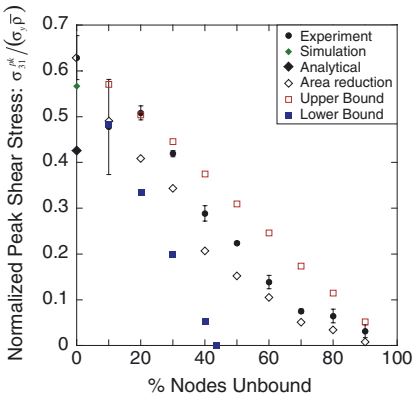

Fig. 17. Normalized peak shear stress with estimated bounds based on effective core area.

6.3.2. Peak shear stress

The experimentally determined peak stresses, for all configurations, are reported in Fig. 16. For a large proportion of the cores tested, node rupture occurred just prior to the true peak stress. Even so, the analytical prediction, assuming a fixed strut end condition (k=2), underestimates the peak strength, as was the case for cores in compression. The measured peak strength for a perfect core is consistent with results reported by Zok et al. (2004). In light of this, the reduced area estimation was calculated using the measured value of peak strength for the fully bound core. This estimation under predicts the peak stress because it completely eliminates contributions from ligaments connected to unbound nodes. At large strains however, unbound nodes were observed to expand or collapse (increase or decrease the bend angle at the node) as the core deformed, contributing to the peak stress response. The experiments also show that the peak stress is significantly affected by the presence of unbound nodes. Both bounds follow a steep linear trend showing that unbound nodes result in a rapid reduction of the peak stress response (Fig. 17).

7. Concluding assessment

This study examines the mechanical response of the pyramidal lattice truss in the presence of imperfections. The imperfections studied are in the form of unbound nodes; a plausible defect that can occur during the manufacturing or loading of these structures. Cores were fabricated using a perforate/bend technique and the mechanical response in the presence of these imperfections was obtained via compression and shear experi-

ments. Finite element simulations were created to model the elastic response and results were compared with the experimental study.

A key finding of the study is that the mechanical response of these structures is not only influenced by the percentage of unbound nodes, but also by their location. Upper and lower bounds can be established based on unbound node connectivity and edge node constraints. Of critical importance for a truss core in compression is the influence of edge nodes on the response. Ideal compressive properties are maintained if edge nodes remain bound to the face sheets. This prevents lateral movement of perimeter nodes during compression and maintains an equiaxed force on the interior nodes. If this requirement is met, the panel can continue to be used in the presence of these imperfections. During the fabrication of sandwich panels, edge constraints can be ensured with the addition of raised node stops placed around the perimeter. They would only have to be tall enough to stop the lateral movement of unbound edge nodes, maintaining the open cell characteristics of the truss core panel. The minor increase in relative density would be offset by the additional safety provided. The lower bound of the compressive response is obtained by debonding successive perimeter nodes.

Compression results, for all random node orientations tested and simulated, show that the pyramidal core is able to sustain adequate stiffness and peak strength properties in the presence of up to approximately 20% unbound nodes. With a small number of unbound nodes the probability that most will be on the edge is unlikely. It is also unlikely that most of the unbound nodes will cluster together with an edge node, given the possible orientations. The response will tend to be near the upper bound due to the probability that several nodes will experience a hydrostatic force.

However, shear properties are significantly degraded upon the introduction of unbound nodes. Each unbound node constitutes a volume of core material that no longer contributes to the response. A model was introduced to predict the reduction of core properties based on the effective area of core material still contributing to the shear response once braze material is removed. This model accurately predicts the stiffness but over estimates the peak stress due to non-negligible contributions from unbound nodes at large strains. Upper limits, calculated using the maximum effective area ratio, illustrate that even for the best case scenario there is a rapid reduction in shear properties. The lower bound is obtained through the minimum effective area ratio. For panels that transfer shear to the core (i.e. panel bending), unbound nodes quickly cause a critical reduction of core shear properties and must be addressed immediately. It is not possible to contain the effects of unbound nodes on shear properties by ensuring that other nodes are bound (i.e. perimeter nodes of a core in compression).

Further effort is needed to develop models that accurately capture the inelastic core properties. Additionally, the influence of nodal constraint and friction must be studied, although from the results presented here it is believed that at least 50% of unbound nodes is required to notice their impact. This study must also be expanded to look at different core topologies. Imperfection sensitivity of sandwich panels under different load orientations is also of interest. Investigating sandwich beams in bending will give insight into the interaction of core compressive and shear properties in the presence of unbound nodes.

Acknowledgements

Russell Biagi and Hilary Bart-Smith gratefully acknowledge the support of the Office of Naval Research through award N00014-06-1-0509. The authors would also like to thank Dr. V. Deshpande for insightful discussions on this topic and Drs. H.N.G. Wadley and D. Queheillalt for use of fabrication facilities and the schematics in Figs. 2 and 3.

References

Abaqus (2002). Abaqus User's Manual. Providence, RI.

Allen, H.G., 1969. Analysis and Design of Structural Sandwich Panels. Pergamon Press, Oxford.

Ashby, M.F., Evans, A.G., Fleck, N.A., Gibson, L.J., Hutchinson, J.W., Wadley, H.N.G., 2000. Metal Foams: A Design Guide. Butterworth Heinemann, Woburn, MA.

ASTM (2000). ASTM International C 273-00, Standard Test Method for Shear Properties of Sandwich Core Materials.

ASTM (2000). ASTM International C 365-00, Standard Test Method for Flatwise Compressive Properties of Sandwich Cores.

Bart-Smith, H., Hutchinson, J.W., Evans, A.G., 2001. Measurement and analysis of the structural performance of cellular metal sandwich construction. International Journal of Mechanical Sciences 43 (8), 1945–1963.

Biagi, R., 2006. Imperfection Sensitivity of Metallic Lattice Truss Structures: Single Layer Pyramidal Core Panels. Mechanical and Aerospace Engineering, University of Virginia.

Bitzer, T., 1997. Honeycomb Technology. Chapman & Hall, London.

Chen, C., Lu, T.J., Fleck, N.A., 1999. Effect of imperfections on the yielding of two-dimensional foams. Journal of the Mechanics and Physics of Solids 47 (11), 2235–2272.

Chen, C., Lu, T.J., Fleck, N.A., 2001. Effect of inclusions and holes on the stiffness and strength of honeycombs. International Journal of Mechanical Sciences 43 (2), 487–504.

Chiras, S., Mumm, D.R., Evans, A.G., Wicks, N., Hutchinson, J.W., Dharmasena, K., Wadley, H.N.G., Fichter, S., 2002. The structural performance of near-optimized truss core panels. International Journal of Solids and Structures 39 (15), 4093–4115.

Christensen, R.M., 2000. Mechanics of cellular and other low-density materials. International Journal of Solids and Structures 37 (1–2), 93–104.

Deshpande, V.S., Fleck, N.A., 2001. Collapse of truss core sandwich beams in 3-point bending. International Journal of Solids and Structures 38 (36-37), 6275–6305.

Deshpande, V.S., Fleck, N.A., Ashby, M.F., 2001. Effective properties of the octet-truss lattice material. Journal of the Mechanics and Physics of Solids 49 (8), 1747–1769.

Evans, A.G., Hutchinson, J.W., Ashby, M.F., 1998. Multifunctionality of cellular metal systems. Progress in Materials Science 43 (3), 171–221.

Evans, A.G., Hutchinson, J.W., Fleck, N.A., Ashby, M.F., Wadley, H.N.G., 2001. The topological design of multifunctional cellular metals. Progress in Materials Science 46 (3-4), 309–327.

Fleck, N.A., Deshpande, V.S., 2003. The Resistance of Clamped Sandwich Beams to Shock Loading. Journal of Applied Mechanics 71 (3), 386–401.

Gibson, L.J., Ashby, M.F., 1997. Cellular Solids: Structures and Properties. Cambridge University Press, Cambridge, UK.

Grimmett, G., 1999. Percolation. Springer, Berlin.

Gu, S., Lu, T., Evans, A., 2001. On the design of two-dimensional cellular metals for combined heat dissipation and structural load capacity. International journal of heat and mass transfer 44 (11), 2163–2175.

Queheillalt, D.T., Wadley, H.N.G., 2005a. Cellular metal lattices with hollow trusses. Acta Materialia 53 (2), 303–313.

Queheillalt, D.T., Wadley, H.N.G., 2005b. Pyramidal lattice truss structures with hollow trusses. Materials Science and Engineering A–Structural Materials Properties Microstructure and Processing 397 (1–2), 132–137.

Rathbun, H.J., Radford, D.D., Xue, Z., He, M.Y., Yang, J., Deshpande, V.S., Fleck, N.A., Hutchinson, J.W., Zok, F.W., Evans, A.G., 2005. Performance of metallic honeycomb-core sandwich beams under shock loading. International Journal of Solids and Structures 43 (6), 1748–1763.

Shanley, F.R., 1967. Mechanics of Materials. McGraw-Hill, New York.

Stauffer, D., Aharony, A., 1992. Introduction to Percolation Theory. Taylor and Francis, London.

Sugimura, Y., 2004. Mechanical response of single-layer tetrahedral trusses under shear loading. Mechanics of Materials 36 (8), 715–721.

Sypeck, D.J., Wadley, H.N.G., 2002. Cellular metal truss core sandwich structures. Advanced Engineering Materials 4 (10), 759–764.

Wadley, H.N.G., Fleck, N.A., Evans, A.G., 2003. Fabrication and structural performance of periodic cellular metal sandwich structures. Composites Science and Technology 63 (16), 2331–2343.

Wallach, J.C., Gibson, L.J., 2001. Defect sensitivity of a 3D truss material. Scripta Materialia 45 (6), 639–644.

Wallach, J.C., Gibson, L.J., 2001. Mechanical behavior of a three-dimensional truss material. International Journal of Solids and Structures 38 (40-41), 7181–7196.

Wicks, N., Hutchinson, J.W., 2001. Optimal truss plates. International Journal of Solids and Structures 38 (30–31), 5165–5183.

Wicks, N., Hutchinson, J.W., 2004. Performance of sandwich plates with truss cores. Mechanics of Materials 36 (8), 739–751.

Xue, Z., Hutchinson, J.W., 2004. Constitutive model for quasi-static deformation of metallic sandwich cores. International Journal for Numerical Methods in Engineering 61 (13), 2205–2238.

Zok, F.W., Rathbun, H.J., Wei, Z., Evans, A.G., 2003. Design of metallic textile core sandwich panels. International Journal of Solids and Structures 40 (21), 5707–5722.

Zok, F.W., Waltner, S.A., Wei, Z., Rathbun, H.J., McMeeking, R.M., Evans, A.G., 2004. A protocol for characterizing the structural performance of metallic sandwich panels: application to pyramidal truss cores. International Journal of Solids and Structures 41 (22–23), 6249–6271.